Numerical simulations of thermal convection at high Prandtl numbers

G. Silano[1], K.R. Sreenivasan[1] and R. Verzicco[2]

[1] International Centre for Theoretical Physics, Trieste - Italy
[2] DIM, Università degli Studi di Roma 'Tor Vegata', Roma - Italy

In this paper we present some results of an extensive campaign of direct numerical simulations of Rayleigh-Bénard convection at high Prandtl numbers ($10^0 \leq Pr \leq 10^4$) and moderate Rayleigh numbers ($10^5 \leq Ra \leq 10^9$). In particular, we examine the Nusselt and the Reynolds number dependences on Ra and Pr. A short discussion on the characteristic flow velocity is also presented.

1 Introduction

The paradigm of thermal convection is the flow between infinitely conducting parallel plates heated from below and cooled from above. This model, called the Rayleigh-Bénard convection, is governed by two non-dimensional parameters: the Rayleigh number $Ra = g\alpha\Delta T h^3/(\nu\kappa)$ and the Prandtl number $Pr = \nu/\kappa$, where g is the acceleration of gravity, h is the fluid layer depth, ΔT is the temperature difference and the fluid properties α, ν and κ are, respectively, the thermal expansion coefficient, kinematic viscosity and thermal diffusivity. The Rayleigh-Bénard model is generally based on the Boussinesq approximation, in which the fluid properties are assumed to be constant despite the temperature gradient across the fluid depth, and the only effect of the temperature in the momentum equation is to modify the buoyancy term.

The influence of the Prandtl number on thermal convection dynamics is difficult to investigate experimentally, because Pr can be substantially changed only by changing the fluid. Examples of studies following this approach can be found in [1] and [2]. A different strategy for varying Pr was adopted in [3], [4] and [5]. It consists of working close to the critical point of compressed gas. This technique enables the exploration of the influence of Pr variations at quite high Ra numbers. However, in both strategies complications arise from the great difficulty of maintaining constant properties across the fluid depth, with consequent violation of the Boussinesq approximation, especially at high Pr numbers.

Numerical simulations can completely overcome these issues, even if they face other kinds of difficulties such as adequate spatial resolution and the integration of long enough time evolutions. Some numerical studies deal with varying Pr numbers ([6], [7], [8], [9], [10]). Only few of them ([7], [10]) mimic a set-up similar to experiments, thus allowing a proper comparison of the results. A smaller number of studies concerns very high-Pr regimes. On the other hand, in [10] the discussion is mainly focused at lower Pr regimes ($2.2\times10^{-3} \leq Pr \leq 15$). In [7] a wider range of Pr numbers is explored ($10^{-3} \leq Pr \leq 10^{2}$), but only at fixed $Ra = 10^{6}$.

We propose a numerical study of thermal convection at high-Pr regimes and moderate Ra numbers for a wide range of Pr and Ra (see figure 1(a)). Numerical simulations at high Pr are very challenging. They require highly refined grids to solve the smaller temperature scales of the flow and large time windows to attain the steady state for mean quantities and to correctly represent the statistics of the slow dynamics of the flow.

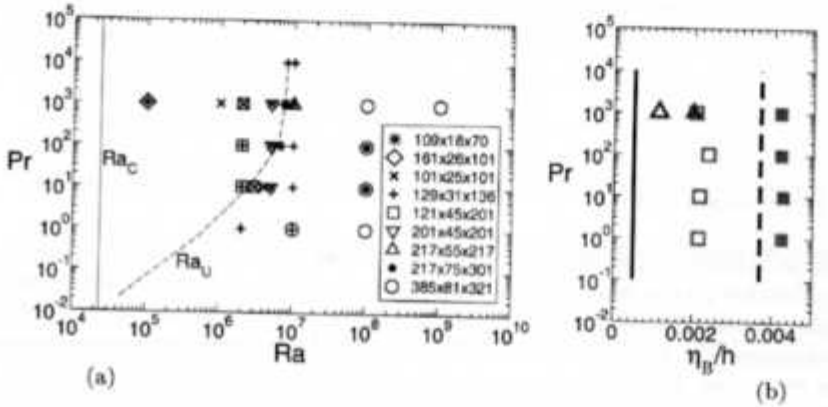

Fig. 1. (a) Map of the performed simulations in a cylindrical cell of aspect ratio $\Gamma = 1/2$. The legend shows the corresponding number of grid points in the azimuthal, radial and vertical directions. The vertical solid line represents the critical Ra for the onset of convection ([11]). The dashed line represents the threshold Ra to pass from steady to unsteady flow. (b) Batchelor scale $\eta_B/h = \left[1/(Re^3\epsilon)\right]^{1/4} \cdot Pr^{-1/2}$ as a function of Pr. Squares: $Ra = 10^8$, upright triangles: $Ra = 10^9$; filled symbols: η_B/h based on $\langle\epsilon\rangle_{V,t}$ (average in space and time); unfilled symbols: η_B/h based on $max\,\langle\epsilon\rangle_t$ (average only in time); vertical solid and dashed lines: respectively minimum and maximum grid size $\Delta = (2\pi r\Delta\theta\Delta r\Delta z)^{1/3}$ for the biggest grid (385x81x321). It is worth noting that the Batchelor scale is quite independent of Pr.

2 Physical and numerical setup

The flow considered here develops in a cylindrical cell of aspect ratio (diameter to cell height) $\Gamma = 1/2$. Cold and hot temperatures are imposed, respectively,

on the top and bottom plates. The sidewall is adiabatic and all the boundaries satisfy the no-slip condition.

The flow is solved by numerically integrating the three-dimensional unsteady Navier-Stokes equations with the Boussinesq approximation. To solve these equations a code ([12]) based on second-order accurate finite-difference schemes on a staggered mesh in cylindrical coordinates and an optimized fractional-step method have been used.

The grid size has been chosen to solve the Batchelor scale ([13]) in the bulk (see fig. 1(b) as an example) and $7 - 15$ points have been placed inside the thermal boundary layers. Refinement analysis has been extensively applied (see fig. 1(a)) in order to assess the grid independence of the solutions. In particular, it has been checked that all the quantities considered in this paper, when computed on most refined grids, differed from those of coarser grids by less than 4%[3]. Where possible, the results from the most refined grids have been used.

The simulations have been run for long enough time windows to obtain statistically converged quantities; in particular, after the initial transient was exhausted each simulation was continued for further 1500 time units based on the large-scale flow. This time unit t_c is defined as the time that a fluid particle needs to cross the cell depth with a typical velocity U_c of the large scale structures: $t_c = h/U_c$. The precise definition of U_c, as well as some discussion of it, will be given in subsection 3.2.

3 Results

3.1 Nusselt number

The Nusselts number (Nu) is the non-dimensional measure of the heat flux crossing the layer of fluid and is one of the most important quantities to calculate. Figure 2a shows Nu divided by Ra^{α} as a function of Ra at $Pr = 10^3$. The exponent $\alpha = 1/3$ corresponds to the best power-law fit in the interval $Ra = [10^5 - 10^8]$. This exponent, however, appears to be over-estimated as Ra increases. Including a provisional result at $Ra = 10^9$ and excluding the simulation at $Ra = 10^5$, the best exponent is equal to 0.307. The exponent $\alpha = 2/7$ corresponds to the best fit in the interval $Ra = [2 \cdot 10^6 - 10^7]$. It is worth noting that for all the three exponents, the data depart at most by about 11% with respect to perfect straight lines, except for $\alpha = 2/7$ and $Ra = 10^5$ where the departure exceeds 20%. This scatter is quite small compared to the data usually available in literature. However it is larger than the error bars which are less than 3.5%(hidden by symbols in both the plots of fig. 2).

In the case of the dependence of Nu on Pr at fixed values of Ra (fig. 2b), the deviations from constant values are also around 10%, even if for $Pr \geq 100$

[3] The same result has been obtained also for second order moments of temperature and velocities fields (average in space and time).

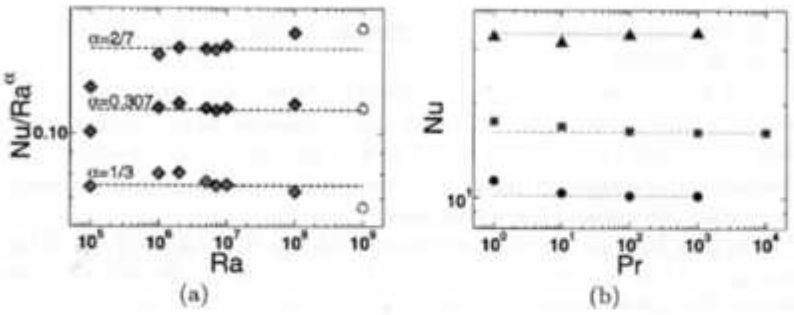

Fig. 2. (a) The Nusselt number, Nu, divided by Ra^{α} versus Ra at $Pr = 10^3$, where α assumes different values. The results at $Ra = 10^9$ are provisional. (b) Nu number versus Pr at $Ra = 2 \cdot 10^6$ (circle), $Ra = 10^7$ (square) and $Ra = 10^8$ (up triangle). The error bars are smaller than the symbols size. The error bar corresponds to the maximum difference of the values obtained computing the Nu number through its relationships with the viscous and the temperature dissipation rate, and averaging the non-dimensional heat flux at each horizontal section of the cell and in the whole volume ([6]).

they fall below about 2%. At $Ra = 2 \cdot 10^6$ and $Ra = 10^7$ we find a trend that decreases slightly with Pr, while at $Ra = 10^8$ the behavior is more scattered. The decreasing behavior is in line with the presence of an overshoot in the Nu versus Pr trend, while passing from low to high Pr regimes ([15]). This trend is confirmed from a running simulation at $Ra = 10^7$ and $Pr = 10^{-1}$. The scattered behavior at $Ra = 10^8$ was not expected. However, a possible explanation lies in differences of the large-scale flow structures found in our simulations. This work is in progress and the results are encouraging.

3.2 Characteristic velocity and Reynolds number

In addition to the Nusselt number, the Reynolds number is an output of the problem reflecting the strength of the flow. For Pr of the order of unity, the typical large-scale velocities of the flow are scaled well by the free fall velocity $U = \sqrt{g\alpha\Delta T h}$ which results from the balance between the inertial term and the buoyancy term of the momentum equation. At high Prandtl numbers, however, the momentum tends to be very diffusive and inertial forces become small; accordingly, the present simulations at high Pr showed that U does not represent the typical velocity of the large scale structures, which is much smaller. By scaling the results from several simulations we have found that the large-scale characteristic velocity is $U_c = U/\sqrt{Pr}$ (note that U and U_c coincide for $Pr = \mathcal{O}(1)$) which yields the estimate of the Reynolds number to be $Re = U_c h/\nu = \sqrt{Ra}/Pr$. As a consequence, the Péclet number becomes $Pe = U_c h/\kappa = \sqrt{Ra}$ independent of Pr. To verify the reliability of this estimates we show the results from two velocities that can be assumed as typical of large scale structures. One is the maximum value of the root-mean-square (rms) of the horizontal velocity profile $U_{rms} = max[\langle u_h^2 \rangle_{A,t}]^{1/2}$, averaged in time and

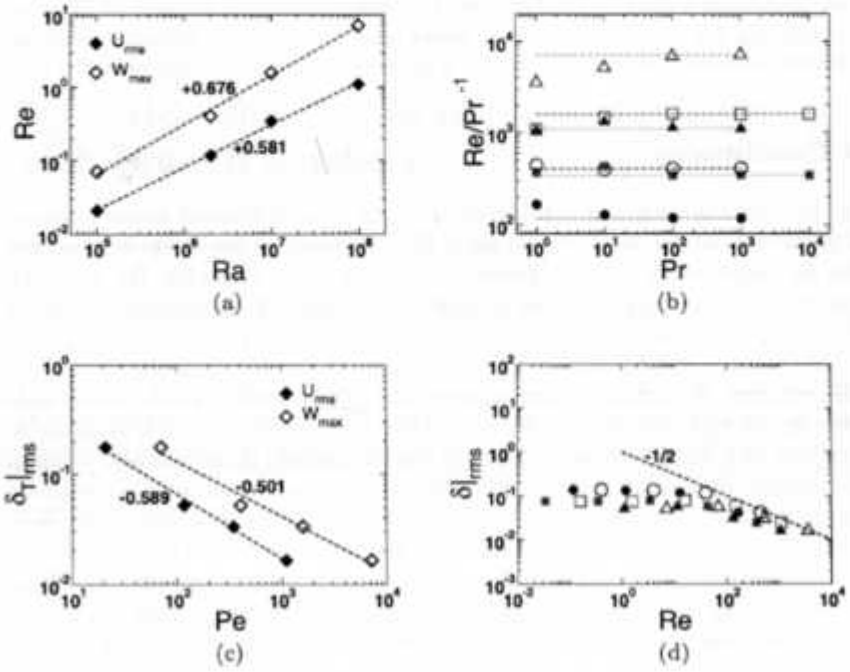

Fig. 3. Filled symbols show Re and Pe based on the rms horizontal velocity U_{rms} and unfilled symbols Re and Pe are based on maximum vertical velocity W_{max}. Diamonds represent trends at fixed $Pr = 10^3$, circles those at fixed $Ra = 2 \cdot 10^6$, squares those at fixed $Ra = 10^7$ and upright triangles those fixed $Ra = 10^8$.

over horizontal surfaces. The other is the time-averaged peak vertical velocity $W_{max} = \langle max[u_z] \rangle_t$.

Figure 3a shows the behavior of Re with respect to Ra at $Pr = 10^3$. The power-law exponent significantly differs for the two velocities and both of them are different from $1/2$. However, it is possible that the exponents closer may be to $1/2$ after the transition from the so-called soft to hard turbulence, as shown in [1]. In the range of Ra numbers explored up to now, no transition is visible. A simulation at higher Ra is presently running.

Figure 3b shows the behavior of Re with respect to Pr at different values of Ra. The Reynolds number is divided by Pr^{-1} to better show the trends. For all Rayleigh numbers and for both choices of typical velocities, the data tend to approach constant values as Pr increases. At $Pr \geq 10^2$ the deviation from a constant value is less than 3.6%. At lower Pr the deviations can exceed 50%, strongly depending from Ra and on the kind of velocity considered.

Finally, figs. 3c and 3d show the behavior of thermal (δ_T) and viscous (δ) boundary layer thickness, respectively, as functions of Pe and of Re. Both of

them are obtained considering the distance from the wall corresponding to the maximum values of rms profiles (of temperature for δ_T and of horizontal velocity for δ). The boundary layers have laminar-like behavior, and the viscous boundary layer saturates to a constant value as Re decreases.

4 Conclusions

In the convective regimes considered here, the Nusselt number seems to follow a power-law of the kind $Nu \sim Ra^{1/3}Pr^0$. However, a lower value exponent for Ra dependency better represents the data trend at higher Ra numbers. Instead, the tendency of Nu to become independent of Pr for large Pr seems to be unambiguous.

As a main result, we have found a $1/\sqrt{Pr}$ correction to apply to the free fall velocity, obtaining a more appropriate representation of the large scale velocity at high Pr. Using this new characteristic velocity, it is possible to derive a new non-dimensional form of the Boussinesq equations and a rough estimation of the Re and Pe numbers that are more suitable at high-Pr analysis than those which derive from the characteristic velocities commonly used to make the equations non-dimensional.

Considering $Nu \sim Ra^{1/3}Pr^0$ and the mean peak vertical velocity W_{max} as the characteristic velocity, the results qualitatively agree with aspects of the Grossmann-Lohse theory ([15]) concerning very high-Pr regimes (III_∞).

We thank CASPUR (www.caspur.it) for providing the computational resources.

References

1. Lam S, Shang XD, Zhou SQ, Xia KQ (2002) Phys. Rev. E 65:066306
2. Ahlers G, Xu X (2001) Phys. Rev. Lett. 86:3320–3323
3. Niemela JJ, Skrbek L, Sreenivasan KR, Donnelly RJ (2000) Nature 404:837–840
4. Roche PE, Castaing B, Chabaud B, Hébral B (2002) Europhys. Lett. 58:693–698
5. Ashkenazi S, Steinberg V (1999) Phys. Rev. Lett. 83:3641–3644
6. Calzavarini E, Lohse D, Toschi F, Tripiccione R (2005) Phys. Fluids 17:055107
7. Breuer M, Wessling S, Schmalzl J, Hansen U (2004) Phys. Rev. E 69:026302
8. Schmalzl J, Breuer M, Hansen U (2002) Goephys. Astrophys. Fluid Dynamics 96:381–403
9. Kerr RM, Herring JR (2000) J. Fluid Mech. 419:325–344
10. Verzicco R, Camussi R (1999) J. Fluid Mech. 383:55–73
11. Oresta P, Stringano G, Verzicco R (2007) Euro. Mech. Flu. 26:1:14
12. Verzicco R, Orlandi P (1996) J. Comput. Phys. 123:402–414
13. Batchelor GK (1959) J. Fluid Mech. 5:113–133
14. Akselvoll K, Moin P (1996) J. Comput. Phys. 125:454
15. Grossmann S, Lohse D (2001) Phys. Rev. Lett 86:3316-3319